STUDY ON THE DETECTABILITY OF BURIED DEFECTS IN CONCRETE STRUCTURES BY USING TRANSIENT INFRARED THERMOGRAPHY FOR HEALTH MONITORING

A. Kamoi[1], M. Yamada[2], Y. Okamoto[3], and S. M. Shepard[4]
[1] Grad. School of Science and Arts, University of East Asia, Shimonoseki, Yamaguchi, Japan; [2] Alae Engineering Co. Ltd., Hannou, Saitama, Japan; [3] Ibaraki National College of Technology, Hitachinaka, Ibaraki, Japan; [4] Thermal Wave Imaging Inc., Ferndale, MI, United States

Abstract: Endurance and safety of concrete structures has recently received a great deal of attention in Japan, as a result of accidents related to falling concrete blocks in railroad tunnels and from highway girders. Sudden forces, such as those generated in an earthquake, or steady state vibrations due to passing of vehicles, may trigger such incidents. However, in either case, air gaps caused by dislodging the reinforcing steel rod accelerate the progression towards catastrophic failure. Aggressive health monitoring to detect hidden defects in concrete structures is essential in order to prevent additional incidents. Conventional inspection techniques, such as ultrasonics and acoustics, have provided only a limited solution to the problem. Infrared thermography has been recently recognized to be a potentially effective NDT methodology for concrete inspection. Infrared thermography is a non-contact technique based on remote sensing of radiation energy from concrete surface, allowing the visualization of concrete surface temperature as two-dimensional thermograms. Since each image covers a relatively large area compared to point scanning ultrasonic or acoustic techniques, thermography provides a fast and practical solution for concrete inspection. This research is devoted to the analysis of the limits of detectability of air defects in mortar using thermography with both external lamp (long pulse) and flash heating, and monitoring temperature distributions on the mortar surface by means of different infrared cameras.

Introduction: The sudden collapse of concrete components in tunnels, highways and bridges has become a serious problem in Japan, where concrete infrastructure is used extensively in mountainous as well as heavily populated areas. As a result, nondestructive detection of hidden defects in concrete infrastructure has become a matter of national importance. Unfortunately, concrete inspection is presently performed using a hammer method that is subjective and time consuming. Infrared Thermography has been identified as a promising technique for rapid detection of hidden defects in concrete. Transient, or active, thermography requires external thermal stimulation of the objects under test by warming up or cooling down the object surface. However, low-power and long heating is significantly affected by environmental conditions [1]. Recent Japanese research in this area has been rather qualitative, i.e. without putting the accent on evaluating parameters of hidden defects [2]. In this study, the experimental results are modeled and processed by using the thermal NDT software package developed at the Thermal Wave Imaging Inc. [3]. This has allowed not only optimizing test parameters but also obtaining reasonable estimates of defect parameters such as size, depth, of air-filled voids and inclusions in concrete [4]. It is shown that this EchoTherm system is the good tool to evaluate health monitoring for buried defects in a surface layer of thick material such as concrete constructions in addition to composite materials like multiple layers and honeycomb of which applications have been already recognized by nearly real time testing mode [5].

Concept of Detection Limit: In this experimental study, the concept of the detection limit in evaluating buried defects in concrete structure is based on the definition of the radiation temperature "difference between the surface radiation temperature over, and far from, a buried defect" as shown in Fig.1 and Fig.2. The radiation temperature over a buried defect （Tc'） is defined by T_{c1}', T_{c2}',T_{c3}', T_{c4}', respectively. The radiation temperature far from buried defects (T_s') is defined by T_{s1}',T_{s2}',T_{s3}', T_{s4}'. In this experimental study four defects buried at different depths have been studied in concrete material. Therefore, each radiation temperature difference between over defect and the surrounding is expressed by Equation 1 to Equation 4 where the buried defect is visualized in the thermograms.

$$\Delta T_{c1}' = T_{c1}' - T_{s1}' = \Delta T_a' \quad (1) \qquad \Delta T_{c2}' = T_{c2}' - T_{s2}' = \Delta T_b' \quad (2)$$

$\Delta T_{c3}' = T_{c3}' - T_{s3}' = \Delta T_c'$ (3) $\Delta T_{c4}' = T_{c4}' - T_{s4}' = \Delta T_d'$ (4)

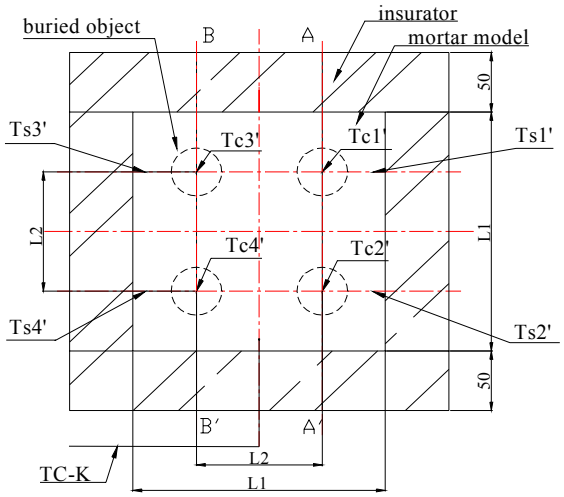

Fig.1 Plane view of concrete structure model

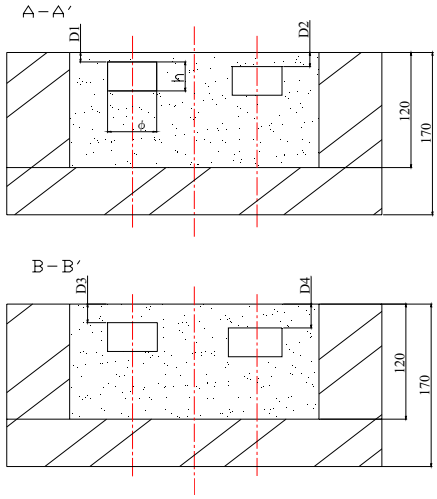

Fig.2 Side view of concrete structure model

In this way, we are able to evaluate the capabilities of infrared thermography in the detection of strange defects buried in soil, concrete, mortar and other materials. The thermal conductivity of mortar and the defect inside are defined as λ_m and λ_d, respectively. Let us consider two cases where a sign of temperature difference is positive or negative:(1) Case: $\lambda_m < \lambda_d$ **:** The heat flux delivered to mortar is more absorbed in defects rather than in the host material. Therefore, the radiation temperature over defects becomes lower than that of surrounding, and the temperature difference becomes negative ($\Delta T_c' < 0$) during heating. (2) Case: $\lambda_m > \lambda_d$ **:** The radiation temperature over defects becomes higher than that of surroundings and the temperature difference is positive ($\Delta T_c' > 0$).

Experimental Apparatus: Figures 3 and 4 show the photographs of experimental apparatus for long pulse heating and halogen heater , respectively. The experimental apparatus for long pulse heating consists of a frame with halogen lamps, concrete model, temperature sensors for the room and mortar surface, oscillographic recorder and an infrared radiometer (IR) with the angle adjuster, lifter, control unit and CRT for IR.The distance from halogen lamps to the mortar surface in the framework can be adjusted from 300 to 500 [mm] in order to change the injected heat flux. The IR camera is mounted on the manual lifter to adjust the camera height and the angle to prohibit the reflection energy from surroundings. The 4 kW halogen lamp unit is made of 4 lamps installed in the reflector made of stainless sheet and its front view is also shown in Fig.4. Figs.5 and 6 show the photographs of experimental apparatus for flash heating and flush lamp heater. The experimental apparatus for flash heating consists of flush lamp food with IR, concrete model where the distance is constant from lamp to concrete surface and control unit for IR and electric supply. The specifications of the two types of IR are shown in Table 1.The concrete model was made of cement, sand and water by the manufacturing steps in the accordance to the standard of Taiheiyo Cement Co. In this experiment the air defect size is Φ40 (diameter) × 20 (height) [mm] and its buried depth is 10, 15, 20 and 25 [mm]. Each depth is corresponding to the letters of a, b, c and d, or 1, 2, 3 and 4, respectively in the sign of the each buried defect. Flash type thermography is “EchoTherm® system” where ® is the registered trademark superscript, manufactured by TWI.

Table 1 Specifications of two types of infrared thermography to be applied

type	material (IR detector)	wavelength [μm]	NETD [˚C]	temperature range [˚C]	IFOV [mrad]
long pulse	HgCdTe (mechanical scan)	NEC:8 ~ 13	0.08 0.02*	– 50 ~ 200	2.0
flash	InSb (focal plane array:FPA)	Indigo:3 ~ 5	0.08 0.025	0 ~ 300	1.5

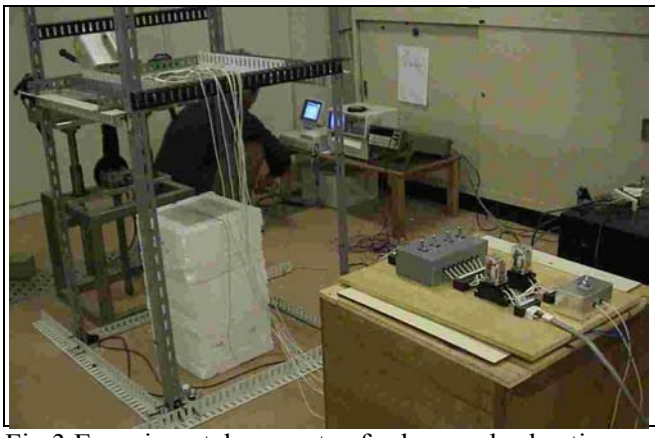

Fig.3 Experimental apparatus for long pulse heating

Fig.4 The front view of halogen lamp unit

Fig.5 Experimental apparatus for flash heating

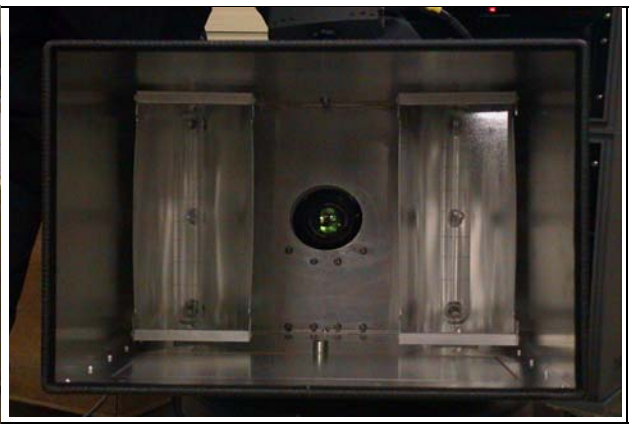

Fig.6 The front view of flash lamp unit with IR

Experimental Method:(1) The atmospheric conditions were monitored and kept constant during experiments. Both the incident J and absorbed αJ heat fluxes [kW/m^2] were determined in the center of the mortar surface by attaching a heat flux meter as shown in Fig. 3 and 5 (here α is the absorption coefficient by 0.6). In both long pulse and flush heating each distribution of heat flux on the surface of concrete model was measured by using heat flux meter**.** In the former case the location of halogen lamps are adjusted to be uniform by changing the distance between the lamps and the mortar surface. The heat flux was 3.12, 3.90, 4.09 [kW/m^2] respectively. And also in the latter case the location of flash lamps are constant and heat fluxr was 55.2, 61.9, 72.4 [kW/m^2] by adjusting the electric power supply in a manner of 50, 75, 100[%] of full power, respectively. (2) Recording thermograms of mortar surface was performed by the following operations:(a) focusing the IR, (b) setting a temperature range, (c) setting a sensitivity range, (d) setting a zoom ratio, (e) choosing a heating time: long pulse heating (15, 30, 60[s]), flash heating (3[ms]), (f) choosing a frame time: long pulse heating (0.2[Hz]), flash heating (1[Hz]), (g) choosing a test time: long pulse heating (130, 150, 240[s]), flash heating (300[s])

Experimental Results: In order to compare with each detection limit in the buried air defects, thermograms of mortar surface were taken by using data due to long pulse and flush heating. Fig.7 (a)~(f) shows the thermograms of the air defects appeared on the mortar surface when long pulse heating of 30 [s] was applied. Square shape image appeared in the center portion of all thermograms is the image of thermocouple to detect surface temperature during the experiment. Image (a) was recorded before heating stage, and image (b) was taken at the end of heating stage. Images (c) to (f) are during the natural cooling stage. The defect areas located over buried air objects looked warmer than the surrounding in the depth(1) of the images (d) to (f) and also the depth(2) of the images (e) to (f). No reverse heat injection from the air defects was observed probably because of quite short time heating compared to conventional long time heating [6]. However, in a conventional experiment, by applying long time heating of the power under 3600 [W/m^2], we observed the change of the radiation temperature difference. In their turn, Fig.8 (a) to (f) shows the thermograms of the air defects by applying the flush heating of 3 [ms]. These thermograms were taken by the first differential treating of those image signals. Here the image (a) was taken before flashing, and the image (b) is just after flashing. Images (c) to (f) were also during the cooling stage. In the case of images (c) to (f) the changes of color in the thermograms were observed like deep to light in color. Those phenomena indicate the existence of air defects in the concrete of the depth (1) of the images (c) to (e) and also the depth (2) of the images (d)

to (e). In the case of flash heating no reverse heat injection was also observed due to the same reason as in the case of long pulse heating.

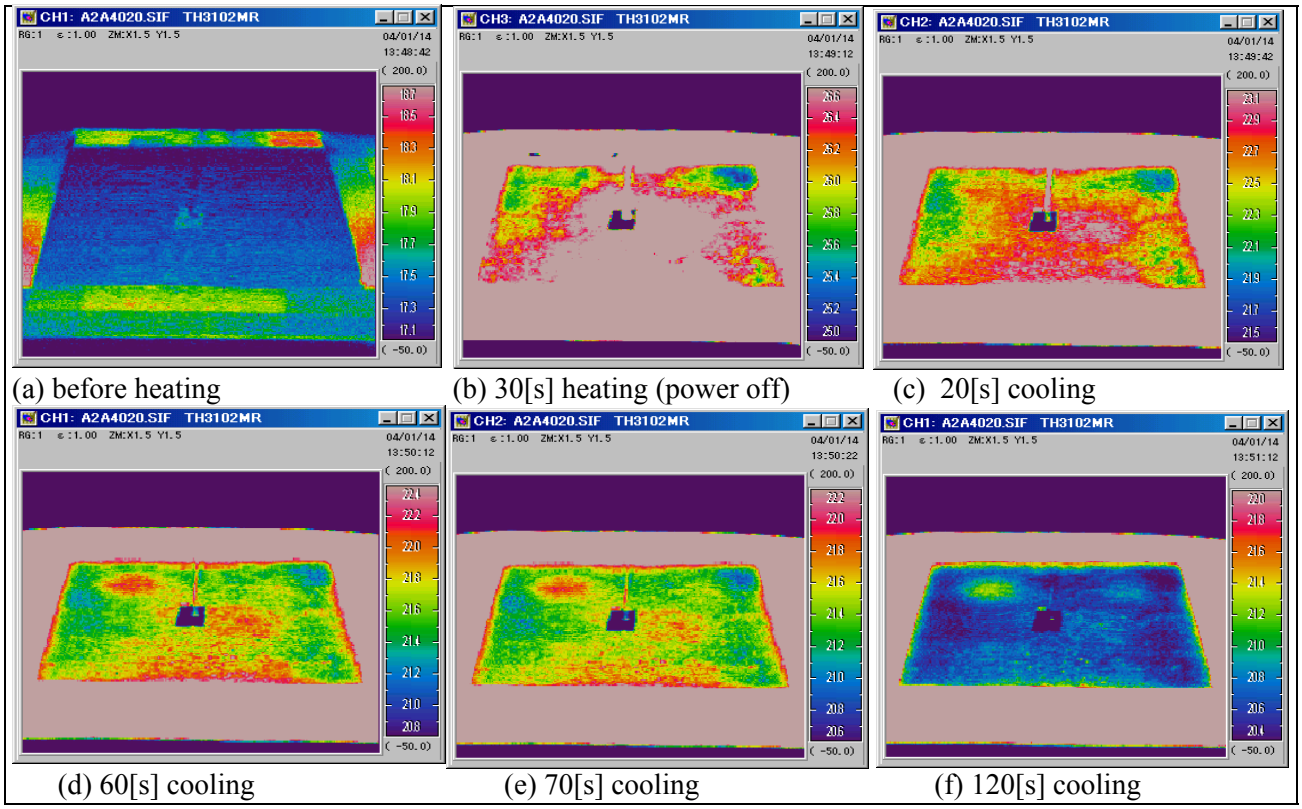

Fig.7 Thermograms taken before and after long pulse heating on the mortar surface by 30 [s] heating, frame time of 0.2 [Hz] and heat flux of 4.09 [kW/m^2]

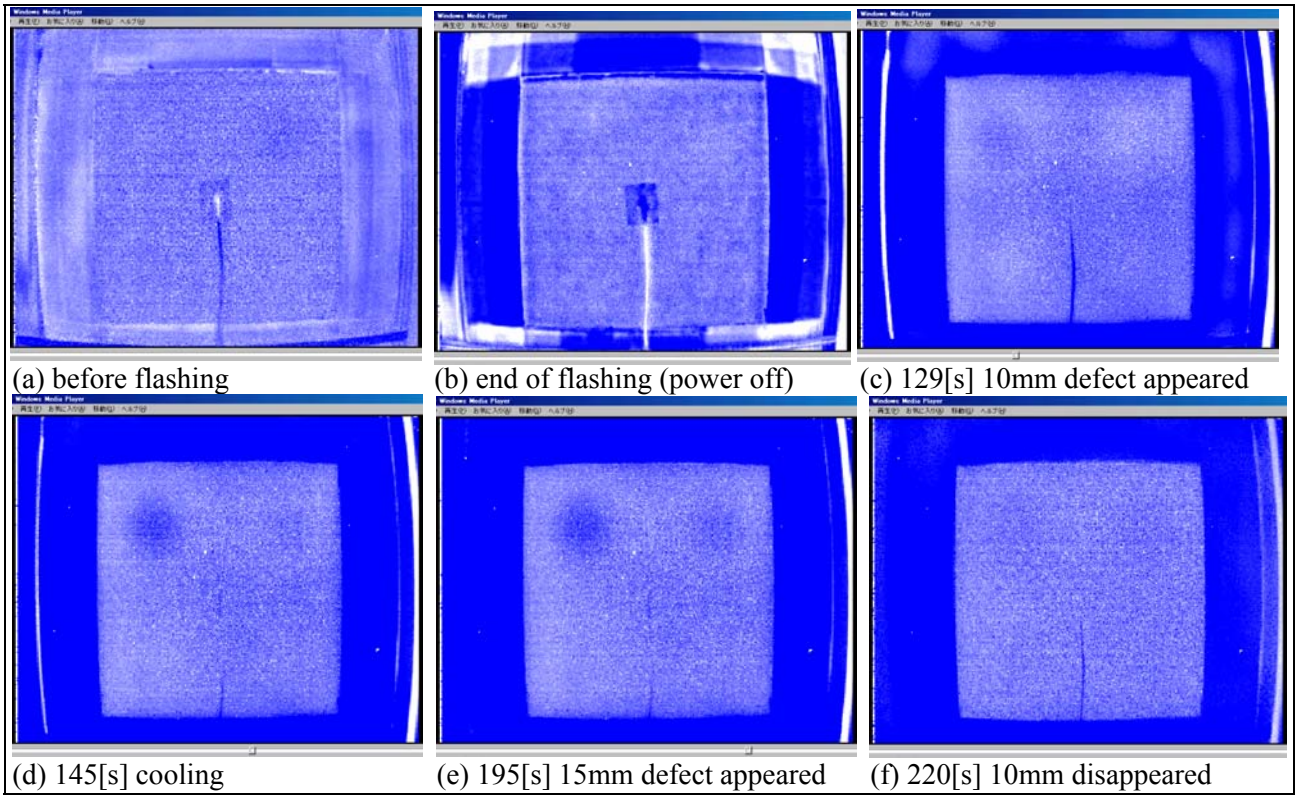

Fig.8 Thermograms taken before and after flash heating on the mortar surface by 3 [ms] heating, frame time of 1 [Hz] and heat flux of 72.4 [kW/m^2]

Discussion of Radiation Temperature Distribution: Fig. 9a) shows the radiation temperature distributions over the air defects of depth 10, 15, 20, and 25 [mm] for 30 [s] long pulse heating, while and also Fig. 9b) shows the results of the same air defects for 3 [ms] flush heating, In both graphs the radiation temperature profiles resemble each other in exponential mode after natural cooling, but the case of flash heating shows fluctuating radiation temperature because of the impulse response as observed in Fig. 9b). This tendency would be due to the expression of high intensity signals instead of radiation temperature.

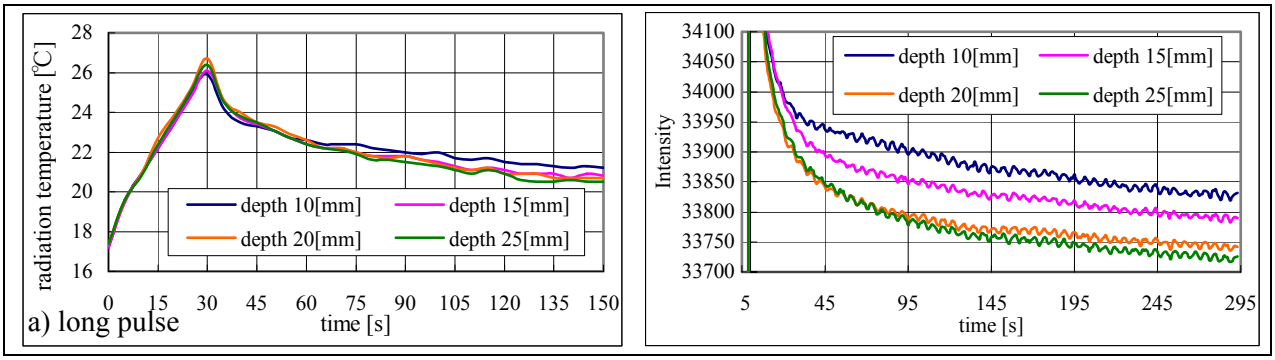

Fig.9 Radiation temperature distributions of long pulse and flash heating

Discussion of Radiation Temperature Difference: Figs.10a) and b) show the behavior of radiation temperature difference and both are scattered in the graphs. In the case of long pulse heating, the scatter of temperature seems to be larger than the case of flash heating. This phenomenon is considered to be due to changing heat exchange between the mortar and the ambient without canceling process of mortar surface roughness in image signal [7]. Each radiation temperature difference ($\Delta T_a'$, $\Delta T_b'$, $\Delta T_c'$, $\Delta T_d'$) shown in the graphs corresponds to the different depth of the buried defect (10, 15, 20, 25 [mm]), respectively. In case of flash heating, the intensity difference does not show regular tendency compared to the case of long pulse heating. This means to be mistaken to select the locations of over and far defect when they were calculated in off line mode after experiment.

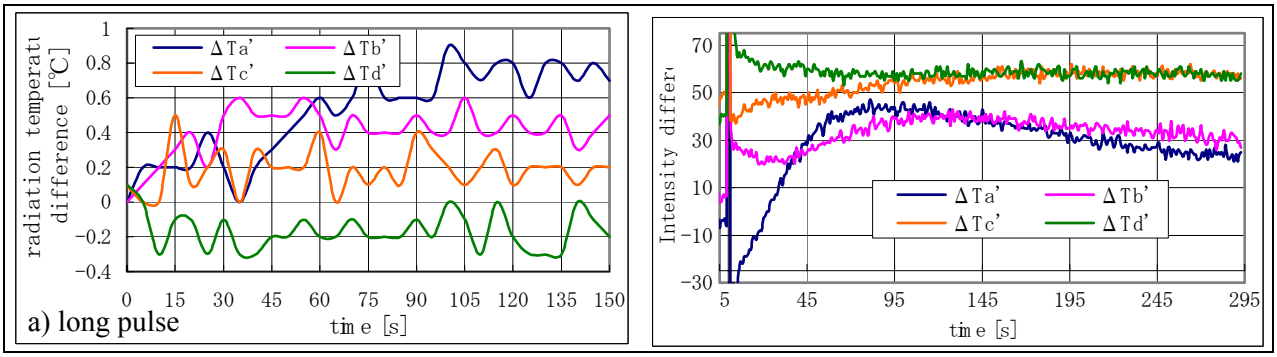

Fig. 10 Radiation temperature difference's distributions of long pulse and flash heating

Discussion of Thermal Images in the Cooling Stage: In the experiment of long pulse heating during 30 [s], the scatter of imaging colors were observed in the thermograms. We believe the detecting capability would be improved if any software is applied for signal processing to make cancelled the image before heating. As the result of additional experiment we found that it will be able to have the chance to detect the inside defects in concrete structures and also other materials, if we take care of cooling effect in the thermograms. That is, the image (c) of 20 [mm] depth will have the chance to be captured after natural cooling of 120 [s]. Therefore, the cooling time should be taken more than three times compared to the heating time in the case of long pulse heating. .In the case of flash heating there is no scatter in the thermogram. Therefore, it is necessary to use the above mentioned software in the conventional infrared thermography.

Discussion of Detection Limit for Visible Air Defects: The detection limit is described and defined by the radiation temperature difference between over and far from the air defect which is appeared and recognized as the defect in the thermogram. In this experiment the detection limit for the air defects are calculated by using Equation (1) to (4) and those results are shown in Fig.11 a) and b). In the case of long pulse heating its range is from 0.1 to 0.5[˚C] and also in the case of flash heating that is from 22 to 40. The detection limit for the air defects have the tendency in which shallow defect is generally larger than deep one in the natural cooling stage. According to consideration of injecting heat flux to the mortar surface, generally speaking, the detection limit for high heat flux is also larger than that for low one. The detectability for air defects is almost

same in the range of full power and three quarter of it.

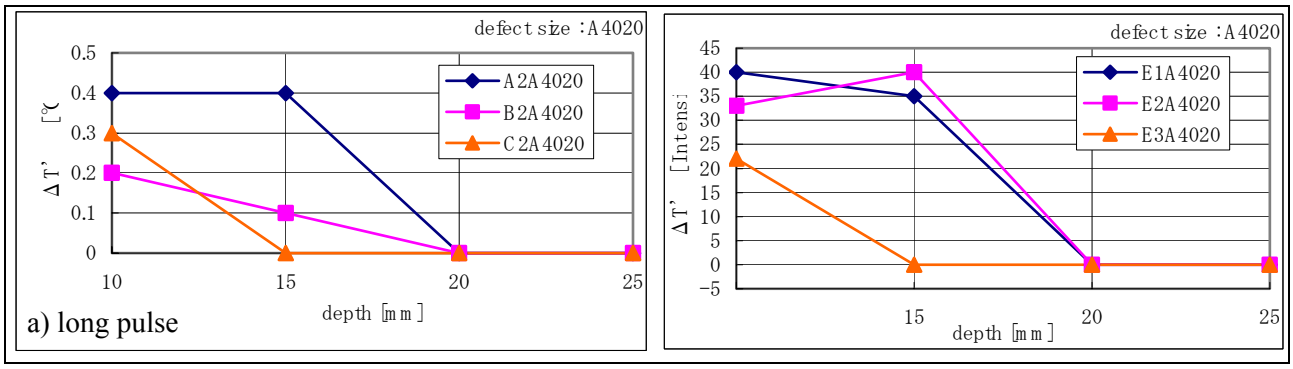

Fig. 11 Detection limit in the case of long pulse and flash heating

Discussion of Comparison Between Long Pulse and Flash Heating Results: In the case of long pulse heating the detection limits for 10 and 15 [mm] depth air defects were determined after 50 and 100 [s] since the experiment was begun. And in the case of flash heating they are also done after 129 and 193 [s] in the same depth of air defects. It is said that time for determination of the detection limit in the case of long pulse heating is faster than the case of flash heating by 61 and 49 [%], respectively. The former was evaluated in the off line of experiment by using the software and it took too much time to get the result. On the contrary, the latter is also done in the on line of experiment by using the software at the same time. Therefore, the latter is very convenient for quick health monitoring. And it is easy to apply the latter as the background noise of mortar surface appeared in the thermograms is also illuminated.

Conclusion: (1) In the case of long pulse heating, any defect was not observed during heating stages of 15, 30 and 60 [s], but air defects of 10 and 15 [mm] were observed in the cooling stage after 50 and 100 [s], respectively..
(2) In the case of flash heating, any defect could be also observed in the cooling stage after 129 and 193 [s], respectively.
(3) Speaking of the time to make visualized air defect of 10 and 15 [mm] depth, the detection limit in the case of long pulse heating is faster than the case of flash heating by 61 and 49 [%], respectively
(4) According as we consider the time to evaluate the detection limit, it is convenient and fast to apply EchoTherm® for the health monitoring.
(5) In the case of long pulse heating the value of detection limit varies from 0.1 to 0.5[˚C], and also from 22 to 40 [intensity] in the case of flash heating. The detection limit of shallow air defect is generally larger than that of deep one in the natural cooling stage.
(6) Cooling time should be at least longer than the heating period in long pulse and flash heating.

References:

[1]. A. Kamoi, Y. Okamot: “Study on Visualization of Thermal Image by Infra red radiometer Influenced by Fluctuations of Environmental Factors”, Journal of Visualization, Vol.5, No.1 (2002), pp. 95-103
[2]. A. Kamoi, T. Kondo, and M. Tanaka: “Study on Detection Limit of Buried Defects in a Mortar by Use of Infrared Radiometer”, Proceeding of JSDNDI Spring Conference-2002 (2002), pp.135-136
[3]. B. Chaudhry, S. M. Shepard, M. Yamada and S. Takahashi; “Advances in Pulsed Thermography”, JSNDI Autumn Conference (2000), pp. 109-110
[4]. A.Kamoi, Y. Okamoto, and V.P.Vavilov: “Studying the inspection limits in detecting buried objects by using infrared thermography”, Proceeding of SPIE, Thermosense XXV, Vol.5073 (2003), pp.339-344
[5]. S. M. Shepard and M. Yamada: Recent Advances in Pulsed Thermography, JSNDI Spring Conference (2004), pp.151-152
[6]. A.Kamoi, Y. Okamoto, and V.P.Vavilov: “Study on Detection Limit of Buried Defects in Concrete Structures by Using Infrared Thermography”, Advances in Nondestructive Evaluation, Proceeding of 11APCNDT (2003), pp.1549-1555
[7]. S. M. Shepard, and T. Ahmed: “Characterization of Active Thermographic System Performance”, Proceeding of SPIE, Thermosense XX1, Vol.3700 (1999), pp.388-392